

Hybrid silicon free-space source with integrated beam steering

J. K. Doylend, M. J. R. Heck, J. T. Bovington, J. D. Peters, M. L. Davenport, L. A. Coldren, and J. E. Bowers

ECE Dept., Univ. of California, Santa Barbara (United States)

ABSTRACT

Free-space beam steering using optical phase arrays are desirable as a means of implementing Light Detection and Ranging (LIDAR) and free-space communication links without the need for moving parts, thus alleviating vulnerabilities due to vibrations and inertial forces. Implementing such an approach in silicon photonic integrated circuits is particularly desirable in order to take advantage of established CMOS processing techniques while reducing both device size and packaging complexity.

In this work we demonstrate a free-space diode laser together with beam steering implemented on-chip in a silicon photonic circuit. A waveguide phased array, surface gratings, a hybrid III-V/silicon laser and an array of hybrid III/V silicon amplifiers were fabricated on-chip in order to achieve a fully integrated steerable free-space optical source with no external optical inputs, thus eliminating the need for fiber coupling altogether. The chip was fabricated using a modified version of the hybrid silicon process developed at UCSB, with modifications in order to incorporate diodes within the waveguide layer as well as within the III-V gain layer. Beam steering across a 12° field of view with $\pm 0.3^\circ$ accuracy and $1.8^\circ \times 0.6^\circ$ beam width was achieved, with background peaks suppressed 7 dB relative to the main lobe within the field of view for arbitrarily chosen beam directions.

Keywords: silicon photonics, LIDAR, free-space communication, optical phased array, laser, hybrid silicon, integrated optics, beam steering, photonic integrated circuit

1. INTRODUCTION

The ability to steer and shape a beam in free space is of interest for a wide range of applications. One application of especial note is light detection and ranging (LIDAR), which provides images at higher resolution than is possible with radar together with the capability to penetrate forest canopy and other obscurants such that hidden landmarks, vehicles, and personnel may be located and identified without sacrificing resolution by resorting to long-wavelength microwave radar [1]. Another application of particular interest is point-to-point free-space communication links, in which beam steering may be used either to select specific recipients for targeted burst transmissions or to maintain a link between non-stationary entities such that low bit-error-rate transmission is maintained despite location shift/sway (e.g. links between buildings) or even significant positional change (e.g. inter-satellite communication). In either case, beam steering using adaptive optics generally requires the use of mechanically moving parts which are therefore subject to degradation in performance from inertial forces and vibrations as well as being susceptible to mechanical wear.

1.1 Optical phased arrays and photonic integrated circuits

Optical phased arrays can be used to steer and shape a beam in free space without mechanical motion [2], and have been demonstrated as such both for LIDAR [3] and for free-space communication links [4], however this approach has largely been implemented thus far using bulk optical components which must be assembled, aligned, and co-packaged. An integrated optical approach in which all optical components are contained within a photonic integrated circuit offers several key advantages over bulk optical assemblies:

- (1) Size. Since individual components are not coupled via either optical fiber or lens assemblies and do not require individual mechanical mounts, space can be devoted solely to a single mount for a chip which contains all required optical components within it, thus saving both volume and weight.

- (2) Optical alignment: since the optical components are fabricated together, optical alignment is accomplished by routing planar waveguides between components on-chip using standard lithography with nanometer-scale tolerances and without the need for independent alignment of micro-optical elements or optical fibers, thus both saving cost and improving system performance.
- (3) Tolerance of vibration and mechanical shock. With optical alignment determined by on-chip fabrication rather than lenses and optical fiber, vibration and mechanical shock poses less of a risk to optical alignment since there are no mechanically-affixed components which can be shifted or shaken loose within the beam path.
- (4) Packaging cost. By eliminating the need to separately assemble and align individual optical components as well as the need for robust mechanical sub-assembly fixtures to hold optical components in place relative to each other, overall packaging cost can be reduced. Additionally, since the photonic integrated circuit can be encapsulated as a single chip, robust functionality in adverse conditions involving particulates and moisture can be achieved without resorting to hermetic packaging.

1.2 Silicon photonics for optical phased arrays

Optical phased arrays can be realized in photonic integrated circuits (PICs) using silicon photonics, thus taking advantage of the fabrication processes and facilities already in widespread use within the electronics industry. Such PICs have been demonstrated using passive silicon waveguides/splitters and gratings together with resistive heaters for thermo-optic control [5][6][7] on silicon-on-insulator (SOI), but this approach necessitates an off-chip source laser which is coupled to the chip via either optical fiber or micro-optics and which must be co-packaged with the chip after being optically aligned, thus diminishing the advantages of using a PIC in the first place (although still vastly preferable, from a packaging standpoint, to aligning/co-packaging the much larger number of components that were thus successfully integrated on-chip). Furthermore, since optical coupling from fiber to SOI involves a large index mismatch, reflections and losses at the interface are inevitable. Optical propagation and scattering losses within the PIC are also inevitable, and the optical phased array itself cannot emit all power into the main beam lobe with 100% efficiency.

It is therefore preferable to have a means of amplifying on-chip light rather than relying on huge input power coupled from a fiber at a single input. Such a capability also offers the additional advantage of providing a means to compensate for phase-dependent losses which must necessarily be introduced on-chip as a result of fast phase-modulation techniques such as carrier-injection and carrier-depletion should beam sweeping at speeds in excess of that achievable thermo-optically be required. Particularly well-suited to this task is the hybrid silicon platform, in which III-V material is die or wafer-bonded to already-patterned SOI waveguides such that optical modes guided within the silicon layer can be electrically pumped due to their evanescent overlap with quantum wells in the III-V material. This approach enables the integration of gain elements for on-chip amplifiers [8] and lasers [9] without the need for separate optical alignment of these components since they are patterned lithographically in the III-V after bonding to the silicon waveguides. This report describes the design, fabrication, and demonstrated beam-sweeping capability of such a device.

2. CONCEPT

In a standard phased array for two-dimensional beam steering, emitter elements or antennae are arranged in a two-dimensional array and phase adjusted to shape/steer the beam. Free-space emission from waveguides in a planar photonic circuit can be achieved using surface gratings, however, and these have the advantage of functioning as 1D phased arrays in their own right since each grating tooth scatters power from the guided mode with a phase delay determined by the effective index of the mode propagating within the waveguide. As such, the emission from a waveguide surface grating is a line in the far field whose emission angle is dictated by the grating pitch (i.e. period between grating teeth), waveguide effective index, and wavelength according to Eq. (1)

$$\sin \theta = \frac{\Lambda n_{eff} - \lambda}{\Lambda}. \quad (1)$$

By tuning wavelength, therefore, the beam in the far field can be steered in one axis and will automatically be collimated in that axis (subject to the finite length of the emission). An array of such gratings enables two-dimensional beam steering since wavelength determines the beam direction in one axis (henceforth referred to as θ) and relative phase across the grating array determines the beam shape/direction in the other axis (henceforth referred to as ψ). In overall concept the PIC-based optical phased array can be realized using a tunable laser coupled to a beam splitter to separate the beam into N channels, a phase modulator for each channel, and finally a grating emitter for each channel. In practice

it is preferable to amplify the beam after the tunable laser and then separately amplify each channel so as to provide both gain and phase adjustment for each emitter. The initial amplifier after the tunable laser (henceforth referred to as the “preamplifier”) not only increases the power launched into the splitter but also provides an easy means of (a) blanking the beam when output to the far field is not desired, and (b) tailoring the far field output power to compensate for variable on-chip losses (this will be discussed in more detail in the Results section). A schematic of the overall concept is shown in Figure 1.

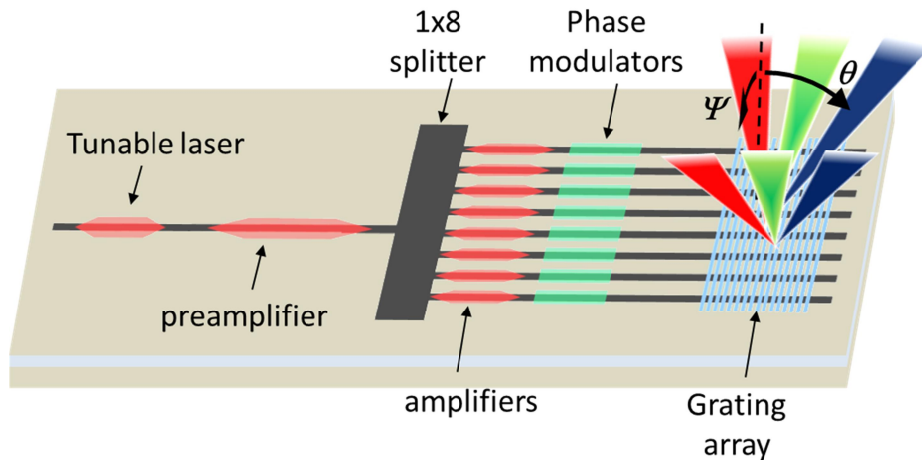


Figure 1. Optical phased array photonic integrated circuit concept. A tunable source laser is followed by a semiconductor optical amplifier (SOA) preamplifier, after which the beam is split into multiple channels (in this case 8). Each channel is separately amplified and phase tuned before being routed to an array of surface gratings. Emission angle of the beam from the surface gratings is determined by wavelength (here symbolized by color) in the θ (longitudinal) axis and by relative phase in the ψ axis.

Because wavelength is used to control steering in one axis and because the shape of the beam in that axis is determined by the grating lithography rather than by active control, an array of N elements requires $2N+1$ controls to steer the beam (N phase controls, N gain controls, and one wavelength control) rather than N^2 as would be required for a standard 2D array architecture, and is therefore inherently more scalable.

3. DESIGN

The design of the system begins with the design of individual components, and for this one must work backward from the beam requirements to arrive at the system capability. In this work the full-width half-maximum (FWHM) beam width goal was $<2^\circ$ with a steering range goal of $>12^\circ$. Since lens optics can in principle be used to expand or contract both the beam and the steering range in a given axis, the true goal was for a minimum of 6×6 (i.e. total steering range divided by beam width) evenly spaced resolvable spots in the far field with a background suppression ratio (i.e. the ratio of the main lobe peak intensity to background peak intensity within the field of view) of 10 dB.

3.1 Channel spacing

The spacing d between channel waveguides determines the angular separation between the main lobe and the side lobes in the far field. With a required separation of 12° to meet the steering range requirement (i.e. one must be able to steer the main lobe by $\pm 6^\circ$ in ψ without causing a side lobe to enter the field of view), the separation between waveguides must not exceed $6.5 \mu\text{m}$ (calculated for 1550 nm wavelength). Note that for this calculation it is not sufficient to maintain a peak-to-peak separation between main lobe and side lobe of 12° ; rather the base of the side lobe exceeding the background suppression must be separated from the main lobe by $>12^\circ$. For the system we chose a channel separation of $5.5 \mu\text{m}$ such that significant background power within the side lobes must fall 14.8° from the main lobe and can be easily aperture without clipping the main lobe at the edges of the field of view.

3.2 Array width and channel count

The lateral width of the overall array (i.e. the product $(N-1)d$, where N is the number of channel waveguides and d is the separation between them) determines the far field beam width in the ψ axis. For far field beam width $<2^\circ$, the array must have a lateral extent $>35 \mu\text{m}$; for d set to $5.5 \mu\text{m}$, $N = 8$. Plots of the calculated side lobe separation vs. waveguide separation and beam width vs. array width are shown in Figure 2.

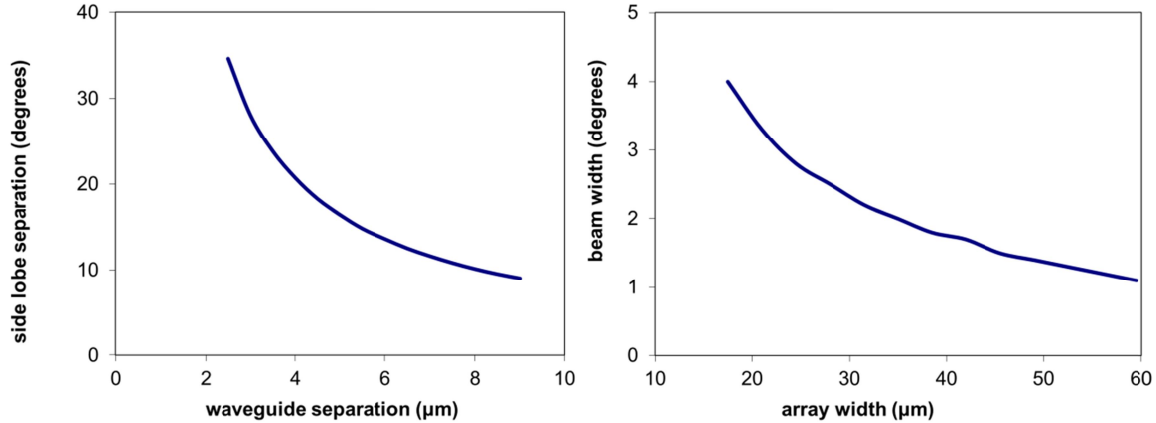


Figure 2. Calculated far field separation between main lobe and base of side lobe (>-10 dB relative to main lobe peak) vs. waveguide separation (left), and calculated far field beam width vs. array width (right).

The longitudinal beam width is determined by the grating strength; for this work the grating emitter used was identical to that reported and characterized in [6], and was thus known in advance to have a beam width of 0.6° .

3.3 Phase modulator design

The phase modulator was designed so as to tune phase thermo-optically by applying forward bias to a $p-i-n$ diode straddling the waveguide. By maintaining large separation between the p and n regions, carrier density within the optical mode was rendered negligible, thus avoiding phase-dependent loss due to free-carrier absorption. The silicon slab between phase modulators was etched to the buried oxide so as to mitigate thermal crosstalk between channels. It should be noted, however, that the measured device exhibited significant output power fluctuations for variations in phase tuning; this was attributed to poor thermal isolation between the phase modulators and the gain elements and will be described in more detail in the Results section. As such, although free-carrier absorption was negligible, the output power was still phase dependent such that the advantage of thermo-optic tuning was largely negated. Subsequent designs therefore employ electro-optic tuning and will be described in a forthcoming report.

Diode dopant profile after ion implantation and annealing was modeled using the Silvaco ATHENA software package, and the current-voltage characteristics and associated carrier densities within the waveguide were modeled using the Silvaco ATLAS software package. Carrier lifetimes within the waveguide for this calculation were assumed to be 0.9 ns in accordance with the data reported by Dimitropoulos et al. [10]. Thermal tuning was predicted to be $57 \text{ mW}/\pi$ using the relation given in Eq. (2):

$$P_\pi = \frac{\lambda \sigma w}{2t \frac{dn}{dT}}, \quad (2)$$

where λ is wavelength, $\sigma = 1.35 \times 10^{-2} \text{ W cm}^{-1} \text{ K}^{-1}$ is the thermal conductivity of the buried oxide [11], w is the effective width of the area over which the heat is dissipated (approximated by the width of the intrinsic region within the diode, or $10 \mu\text{m}$), $t = 1 \mu\text{m}$ is the thickness of the buried oxide, and $dn/dT = 1.86 \times 10^{-4} \text{ K}^{-1}$ [12] is the thermo-optic coefficient of silicon.

The phase modulator cross-section and a plot of expected carrier density vs. bias are shown in Figure 3 for a phase modulator length of 2 mm .

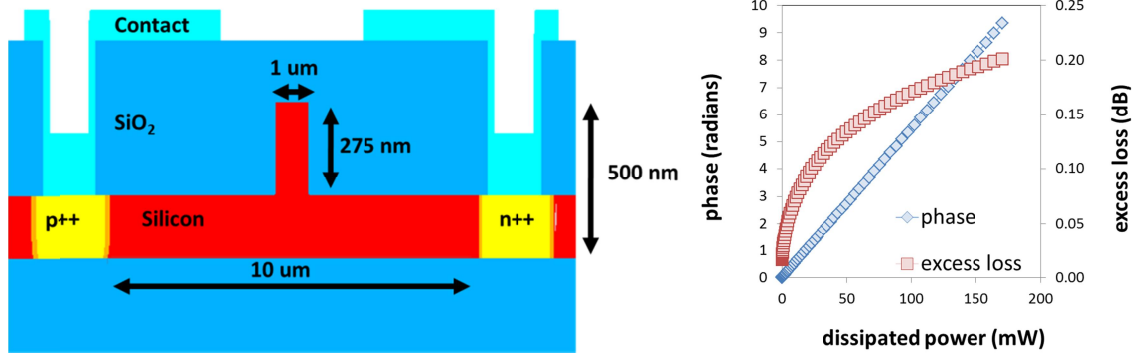


Figure 3. Cross-section of the phase modulator profile (left), and predicted thermo-optic tuning and free-carrier induced excess loss vs. thermal power (right).

3.4 Amplifiers and laser

The gain elements within both the SOA's and the tunable laser were based on the design reported by Kurczveil et al. [13] with the exception of rib waveguide width, which was chosen to be 2.5 μm within the SOA's in order to increase mode volume and hence maximum output power. Length of these elements was chosen to be 2.3 mm (also with the intention of increasing output power), while the preamplifier's length and rib width were chosen to be 1 mm and 2 μm respectively for higher gain/mm. The tunable laser was composed of two bus waveguides each with a gain section, coupled together with ring resonators having circumferences of 400 μm and 420 μm respectively such that their respective transmission spectra would overlap at only one wavelength within the available gain bandwidth. Thermo-optic tuning of the ring spectra by means of resistive heaters overlying them allowed the common transmission peak to be shifted so as to tune the laser. This tunable laser will be described in greater detail in a forthcoming publication.

3.5 Integrated device

The CAD layout of the overall 8-channel device is shown in Figure 4.

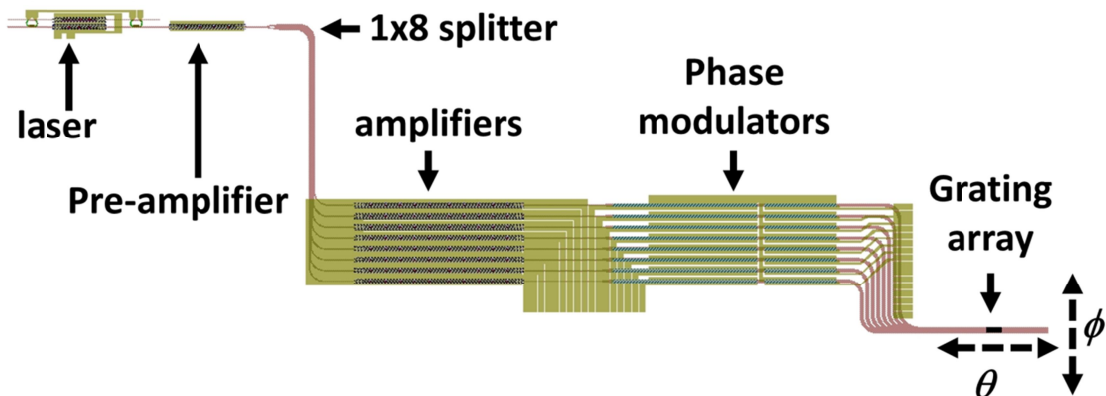


Figure 4. CAD layout of the overall device showing the tunable laser, pre-amplifier, waveguide splitter, channel amplifiers, phase modulators, and grating array.

4. FABRICATION

Silicon-on-insulator (SOI) with 500 nm lightly p-doped ($3 \times 10^{15} \text{ cm}^{-3}$) top silicon and 1 μm buried oxide was used as the starting material. Rib waveguides were patterned and etched to a depth of 275 nm in the SOI. Boron and phosphorus dopants were introduced via ion implantation and a 10 minute 1050°C anneal to form the phase modulators diodes. The grating array for free-space emission was patterned using e-beam lithography and etched to a depth of 50 nm. III-V quantum well laser material was then wafer-bonded to the top silicon surface, after which the bonded chip was lithographically patterned and etched to form diodes within the III-V material to serve as electrically pumped gain

elements. Metal contacts were formed via e-beam evaporation and liftoff. Buffer layers composed of SU8 and PECVD SiO₂ were used over the waveguides to maintain sufficient separation between the overlying metal traces and the waveguides to avoid excess optical losses.

5. RESULTS

5.1 Phase modulators

Phase tuner current-voltage characteristics were used to estimate the effective carrier lifetime, which was determined to be 1.9 ns rather than the expected value of 0.9 ns. Calculations of the associated carrier densities suggested free-carrier absorption of 0.75 dB and free-carrier induced phase shift of -0.8 radians for 100 mW of dissipated i^2R power, degrading the thermo-optic tuning efficiency accordingly. Tuning efficiency was measured on a test structure Mach-Zehnder interferometer and found to be $97 \text{ mW}/\pi$. The measured result together with a fit using the carrier lifetimes derived from the current-voltage characteristic and the measured thermo-optic efficiency is shown in Figure 5.

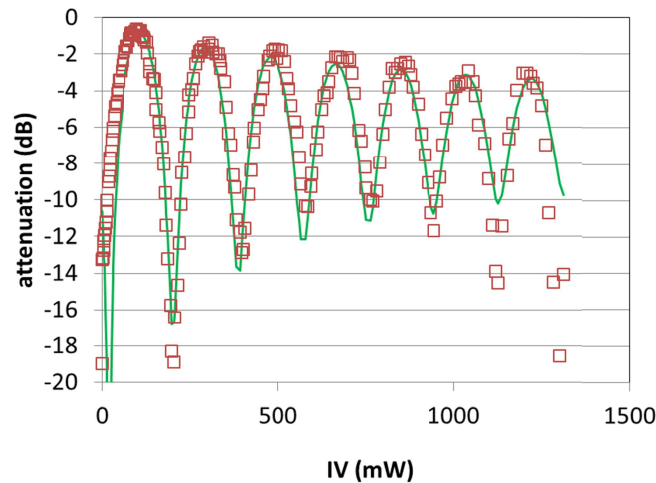


Figure 5. Measured thermo-optically tuned Mach-Zehnder interferometer transfer function to determine the phase tuning efficiency. The fitted curve was calculated using the measured phase-tuning efficiency together with calculated attenuation from free-carrier absorption deduced from the effective carrier lifetime.

5.2 On-chip laser

The on-chip laser within the 8-channel system was not tunable owing to faulty tuner probe pads, however a similar laser on the same chip was measured and found to have 5.5 mW output power, < 7 MHz linewidth, 46 dB sidemode suppression, and 40 nm tuning range (1561 nm to 1601 nm).

5.3 Photonic integrated circuit

The overall device was characterized by recording the beam profile in the far field using an IR camera and imaging lens system and using a feedback algorithm to adjust the phase on each channel with an 8-channel laser driver, similar to the method described in [6]. Power emitted from each channel was first equalized by turning on one channel at a time and observing the intensity of the far field line thus produced on the IR camera. One channel (channel 5) was observed to be faulty and was turned off for the duration of the measurement – this limited the maximum possible background suppression to 8.3 dB within the field of view; 7 dB background suppression was consistently achieved/measured with a beam width of 1.8° in ψ and 0.6° in θ . Due to significant heating of the top silicon layer, the gain from the SOAs was found to be highly dependent on the phase modulator settings. Accordingly the phase modulators and SOAs were cycled at 125 Hz, 20% duty cycle to mitigate on-chip heating. In order to avoid contamination of the observed far field pattern during SOA and phase modulator ramp-up, the preamplifier was used to blank the beam for the first 800 μs of the on-cycle before being turned on for the remaining 800 μs . With the chip mounted on a heat sink held at 18°C , the beam was profiled and steered across the far field at 1° increments from -6° to $+6^\circ$ at a single wavelength. It is noteworthy that with the observed tuning range (40 nm) for the on-chip laser and measured wavelength steering of $0.14^\circ/\text{nm}$ [6], tuning of 5.6° in the longitudinal direction is possible. A plot of measured and predicted beam cross-sections for each

axis is shown in Figure 6, and plots of the beam steered to directions in the far field across a 12° range are shown in Figure 7.

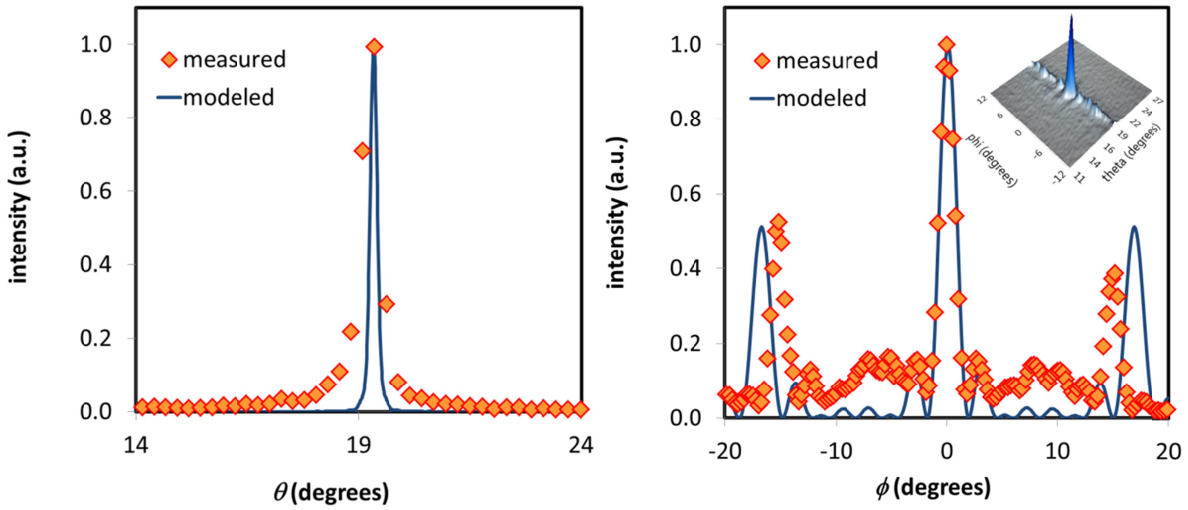


Figure 6. Measured and predicted beam cross-sections in the longitudinal (wavelength-tuned) axis (left) and lateral (phase-tuned) axis (right). The inset shows the 2D profile of the beam measured on an IR camera.

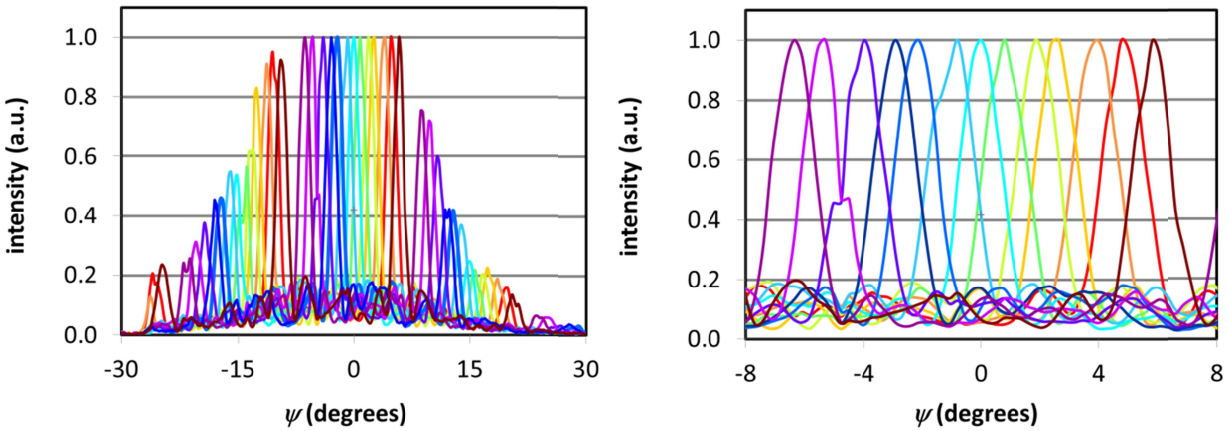


Figure 7. Measured beam profiles in the far field for the beam steered from -6° to +6° showing both the main and side lobes (left) and the aperture field of view (right).

As mentioned above, the beam power was not uniform or even predictable for disparate phase settings / steering angles in the far field owing to the effect of phase tuner heating on the gain elements within the circuit. However it was found that adjusting the preamplifier current preserved the beam shape (i.e. beam width and background suppression) while simultaneously enabling the beam power variations to be completely compensated such that the far field profile could be rendered flat as a function of steering angle. The variation in beam power with and without pre-amplifier adjustment is shown in Figure 8 together with the measured beam profiles for the required range of preamplifier settings.

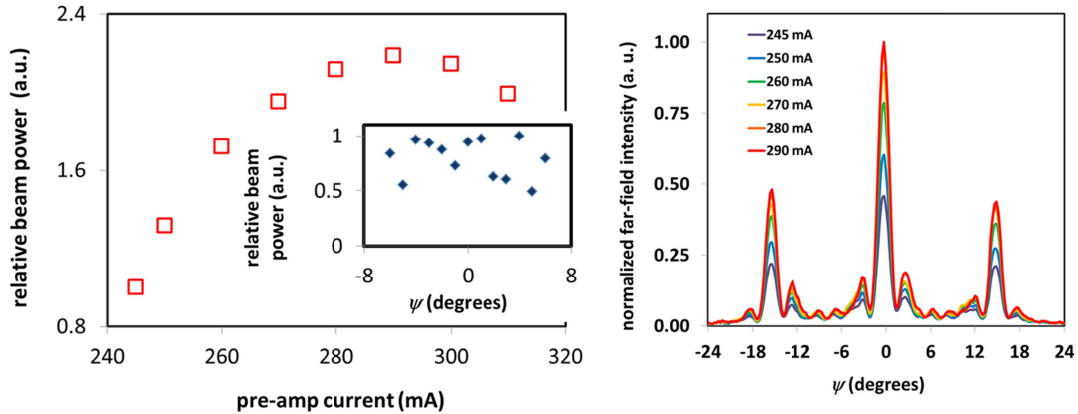


Figure 8. Relative beam power vs. preamplifier current (left) together with relative beam power without pre-amplifier current adjustment (inset left), and beam profiles vs. pre-amplifier current (right).

The beam power was measured by steering the beam to a detector positioned in the far field and found to be $4.1 \mu\text{W}$. Far field linewidth and sidemode suppression were measured by steering the beam to a fiber collimator connected to an APEX 2051A optical spectrum analyzer. Linewidth of the far field output was 36 MHz and sidemode suppression was 30 dB, both somewhat degraded from the characteristics of the standalone laser. This is not surprising given the many sources of feedback into the laser which are present in the integrated device. However the degradation was small enough as to make no significant different to the beam relative to the target metrics of background suppression and beam width in the far field.

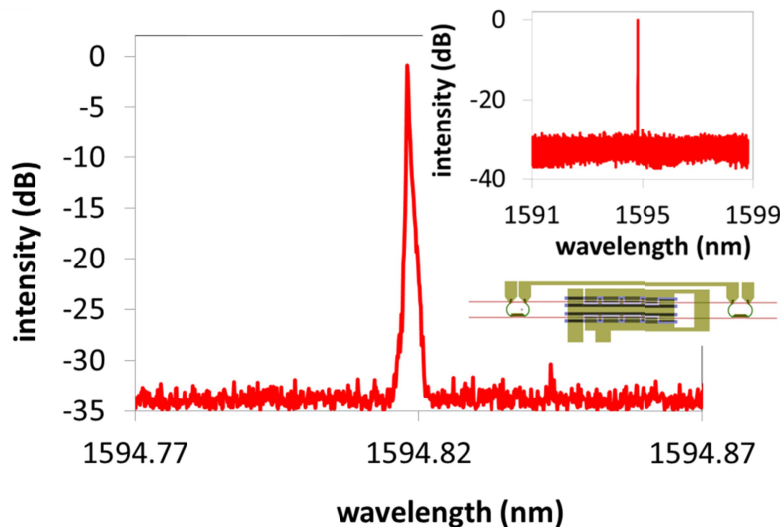


Figure 9. Far field laser spectrum measured on an optical spectrum analyzer. The insets show a broader spectrum to illustrate the suppression of longitudinal modes (upper inset) and a CAD layout of the tunable on-chip laser (lower inset).

6. CONCLUSION

A photonic integrated circuit fabricated according to the hybrid silicon platform has been used to demonstrate a free-space steerable laser using an optical phased array integrated with a tunable laser. The device exhibited 12° phase-controlled steering with $1.8^\circ \times 0.6^\circ$ beam width, and the on-chip laser was shown to be tunable over a range consistent with 5.6° steering in θ for a combined beam steering capability of 7×9 resolvable spots in the far field with 7 dB background suppression.

The authors would like to thank Pietro Binetti, Weihua Guo, Chad Althouse, Scott Rodgers, Josh Conway, and Predrag Milojkovic for useful discussions.

REFERENCES

- [1] Marino, R. M., and Davis, W. R., "Jigsaw: a foliage-penetrating 3D imaging laser radar system," *Lincoln Lab. Journal* 15, 23–36 (2005).
- [2] McManamon, P. F., Bos, P. J., Escuti, M. K., Heikenfeld, J., Serati, S., Huikai, X., and Watson, E. A., "A Review of Phased Array Steering for Narrow-Band Electrooptical Systems," *Proc. IEEE* 97, 1078-1096 (2009).
- [3] Schweinsberg, A., Shi, Z., Vornehm, J., and Boyd, R., "A slow-light laser radar system with two-dimensional scanning," *Opt. Lett.* 37, 329-331 (2012).
- [4] Henderson, C. J., Leyva, D. G., and Wilkinson, T. D., "Free Space Adaptive Optical Interconnect at 1.25 Gb/s, With Beam Steering Using a Ferroelectric Liquid-Crystal SLM," *J. Lightwave Technol.* 24, 1989-1997 (2006).
- [5] Van Acoleyen, K., Rogier, H., and Baets, R., "Two-dimensional optical phased array antenna on silicon-on-insulator," *Opt. Express* 18, 13655-13660 (2010).
- [6] Doylend, J. K., Heck, M. J. R., Bovington, J. T., Peters, J. D., Coldren, L. A., and Bowers, J. E., "Two-dimensional free-space beam steering with an optical phased array on silicon-on-insulator," *Opt. Express* 19, 21595-21604 (2011).
- [7] Sun, J., Timurdogan, E., Yaacobi, A., Hosseini, E. S., & Watts, M. R., "Large-scale nanophotonic phased array," *Nature*, 493, 195-199, (2013).
- [8] Park, H., Kuo, Y.-H., Fang, A. W., Jones, R., Cohen, O., Paniccia, M. J., and Bowers, J. E., "A Hybrid AlGaInAs-Silicon Evanescent Amplifier," *IEEE Photon. Technol. Lett.* 19, 230-232 (2007).
- [9] Fang, A. W., Sysak, M. N., Koch, B. R., Jones, R., Lively, E., Kuo, Y., Liang, D., Raday, O., and Bowers, J. E., "Single-Wavelength Silicon Evanescent Lasers," *IEEE J. Sel. Top. Quantum. Electron.* 15, 535-544 (2009).
- [10] Dimitropoulos, D., Jhaveri, R., Claps, R., Woo, J. C. S., and Jalali, B., "Lifetime of photogenerated carriers in silicon-on-insulator rib waveguides," *Appl. Phys. Lett.* 86, 071115-1 – 071115-3 (2005).
- [11] Lide, D. R., [CRC Handbook of Chemistry and Physics], "Thermal Conductivity of Glasses", CRC Press, Boca Raton, 12-205 – 12-208 (2005).
- [12] McCaulley, J. A., Donnelly, V. M., Vernon, M., Taha, I., "Temperature dependence of the near-infrared refractive index of silicon, gallium arsenide, and indium phosphide," *Phys. Rev. B* 49, 7408-7417 (1994).
- [13] Kurczveil, G., Heck, M. J., Peters, J. D., Garcia, J. M., Spencer, D., Bowers, J. E., "An Integrated Hybrid Silicon Multiwavelength AWG Laser," *IEEE J. Sel. Top. Quantum Electron.* 17, 1521-1527 (2011).